Minimally Invasive Implant Type Electromagnetic Biosensor for Continuous Glucose Monitoring System: In vivo Evaluation

Jagannath Malik, Seongmun Kim, Jong Mo Seo, Young Min Cho, Franklin Bien*, *Senior Member, IEEE*

Abstract*— *Objective: Continuous glucose monitoring system (CGMS) is growing popular and preferred by diabetes over conventional methods of self-blood glucose monitoring (SBGM) systems. However, currently available commercial CGMS in the market is useful for few days to few months. This paper presents a durable, highly sensitive and minimally invasive implant type electromagnetic sensor for continuous glucose monitoring that is capable of tracking minute changes in blood glucose level (BGL). *Methods*: The proposed sensor utilizes strong oscillating nearfield to detect minute changes in dielectric permittivity of interstitial fluid (ISF) and blood due to changes in BGL. A biocompatible packaging material is used to cover the sensor. It helps in minimizing foreign body reactions (FBR) and improves stability of the sensor. *Results*: The performance of the proposed sensor was evaluated on live rodent models (C57BL/6J mouse and Sprague Dawley rat) through intravenous glucose and insulin tolerance tests. Biocompatible polyolefin was used as the sensor packaging material, and the effect of packaging thickness on the sensitivity of sensor was examined in in-vivo test. Proposed sensor could track real-time BGL change measured with a commercial blood glucose meter. High linear correlation ($R^2 > 0.9$) with measured BGL was observed during in vivo experiments. *Conclusion*: The experimental results demonstrate that the proposed sensor is suitable for long term CGMS applications with a high accuracy. *Significance*: Present work offers a new perspective towards development of long term CGM system using electromagnetic based implant sensor. The in vivo evaluation of the sensor shows excellent tracking of BGL changes.

***Index Terms*—Continuous glucose monitoring system (CGMS), glucose sensor, biosensor, in vivo, in vitro, phantoms.**

"This work was supported by the Technology Innovation Program (Development of sustained precision, semi-permanent, and low time lag 3rd generation CGMS for diabetes patients without blood sampling in glucose monitoring, 1415172845, 20011402) funded By the Ministry of Trade, Industry & Energy (MOTIE, Korea)." "This work was supported by the National Research Foundation of Korea (NRF) grant funded by the Korea government (MSIT) (NRF-2017R1A5A1015596)."

J. Malik is with SB Solutions, Seoul 06731, Rep. of Korea. S. Kim and F. Bien are with School of Electrical Engineering, UNIST Ulsan 44919 Rep. of Korea. J. M. Seo is with Dept. of Electrical and Computer Engineering, Seoul National University, Seoul 151-742, and with Dept. of Ophthalmology, College of Medicine, Seoul National University Hospital, Seoul 110-744, Rep. of Korea. Y. M. Cho is with Department of Internal Medicine, Seoul National University College of Medicine, 101 Daehak-ro, Jongno-gu, Seoul, 03080, and with Department of Internal Medicine, Seoul National Univ. Hospital, Seoul, Rep. of Korea. F. Bien is with SB Solutions, Seoul 06731, Rep. of Korea. The First author and second author have contributed equally. (Correspondence email: bien@unist.ac.kr)

I. Introduction

ACCORDING TO International Diabetes Federation (IDF, 2019) survey, 9.3% of the adult population worldwide (approximately 463 million people) suffer from diabetes [1]. Poor blood glucose management in diabetes leads to other health complications [2]. Commercially available glucose monitoring devices are based on finger pricking method. However, this point-of-care invasive lancet approach is painful, does not give insight about the trend of glucose level, and is not economical for patients requiring frequent blood glucose checks (e.g., type-2 diabetes). Active research is going on for the development of effective technique, sensor device to measure BGL accurately and continuously [3], [4]. Techniques that are mostly explored are based on fluorescent activity due to glucose binding [5], optical coherence tomography [6], [7] and infrared spectroscopy [8], [9]. Noninvasive approach to detect glucose using Raman spectroscopy is also reported in [13], [14]. The electrochemical enzyme method [21], [22] and the fluorescence spectroscopy method [23] for glucose detection are the most studied and sold as commercial products. However, the lifetime of these sensors still a pertaining issue. In the case of enzyme-based glucose sensors, the sensitivity is high, but the lifespan is low. So, it needs to be replaced periodically [25]. Fluorescent materials also have a low lifespan and degrades over time, so the long-term use is not possible [26].

Measuring glucose directly from external body fluids, e.g., tear drops, saliva and sweat, is considered a potential alternative to invasive measurement of BGL [15]-[19]. However, measurable glucose quantity is much lower (less than 10%) compared to the actual glucose present in the blood. Thus, measuring glucose from interstitial fluid (ISF) is more promising [20], [24]. The development of minimally invasive and implantable biosensors has opened up window for developing CGMS. Minimally invasive sensor attaches to the body and measures BGL from ISF rather than actual blood. Continuous measurement of glucose level has the advantage of predicting possible hypoglycemic/hyperglycemic events to alert the patient. Few commercial CGMS are already available, however durability of the sensor is still an issue. Application of electromagnetic sensors as non-invasive/invasive implant device got increased attention in biology, medicine, biomedical

engineering, and also proven to be safe for long term in vivo use. Moreover, the electromagnetic properties of these EM-based sensors do not degrade over time, which is highly suitable for long-term use with a sustained accuracy.

The fundamental working principle of these EM-based glucose sensors is to respond towards dielectric permittivity changes due to changes in glucose level [12], [54], [57]. The fact that the dielectric permittivity changes as the concentration of glucose changes in blood over a broad frequency spectrum gives hope for the development of an EM-based glucose sensor [11], [28], [30], [51], [54-58]. Robust and reusable EM-based sensors are previously been explored for blood glucose detection [10], [27]. Often a linear correlation between the sensor frequency and BGL is desirable for successful implementation of EM-based glucose sensor. Some recent developments on electromagnetic-based BGL detection are discussed in [54]-[58]. In [54], dielectric properties of glucose-loaded samples are measured using open ended coaxial probes in a broad frequency span from 300 MHz to 67 GHz. A non-invasive millimeter wave radar made of two Tx and four Rx antennas with high temporal resolution is used for remote detection of glucose concentration in test tubes samples. A proof-of-concept prototype to detect changes in glucose dependent dielectric properties at 60 GHz using Soli alpha kit millimeter-wave radar is presented in [55]. An EM-based glucose measurement sensor using millimeter waves has been reported in [31]. Authors proposed sensing system in which the test sample is placed between two patch antennas aligned and facing each other. The transmission coefficient depends on the dielectric permittivity changes of sample which is correlated to glucose level. The extended results of the work with real time non-invasive BGL measurement from pig's ear is reported in [56]. They concluded glucose tracking efficiency also depends on frequency band, sample thickness, back ground noise level and sensitivity of the receiver. In [57], authors presented a modified microstrip line-based glucose sensors for non-invasive glucose monitoring. The sensor is optimized for improved penetration depth that increased the sensitivity towards glucose dependent permittivity changes. Two frequency bands, 100-500 MHz and 1.4-1.9 GHz were used to validate the sensor performance. In [58], authors designed EM-based glucose measurement system at V-band consisting of two open-ended waveguides. They observed almost linear correlation between glucose concentration and scattering parameters.

Measuring glucose level from ISF and blood vessels using an external sensor is challenging and erroneous due to multiple reflections and strong attenuation from different bio-tissue layers. These layers have different dielectric permittivity levels, e.g., skin is around 30~40, dermis/epidermis is around ~ 40, fat layer is around 5~10, and muscle is around 50~55 [32]. It is difficult to measure blood glucose accurately using an external sensor because the electromagnetic fields are scattered through different layers having different dielectric permittivity levels. Other factors, such as attenuation of the EM signal through a lossy bio-tissue medium, also restrict the successful application of external EM-based sensors. However, using an implantable sensor can overcome these limitations.

In this paper, we propose a compact EM-based resonator as a possible implantable sensor for continuous tracking of BGL. The sensor is intended to be implanted subcutaneously and capable of detecting minute permittivity changes of ISF due to changes in BGL.

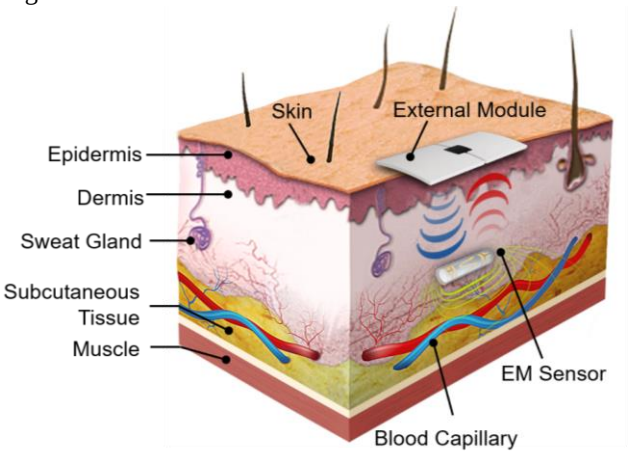

Fig. 1. Illustration of electromagnetic-based sensor for CGM system: subcutaneously implanted EM-based sensor for tracking BGL, and an external module (placed outside on skin just above implant sensor) to send power and receive data from the implant sensor.

Fig. 1 illustrates the conceptual implantation of the proposed sensor into the body with an external module attached outside the body over sensor location. The illustrated anatomy consists of a few centimeters of skin composed of epidermis, dermis, and subcutaneous tissue and muscle. The proposed sensor can be inserted into the dermis and is capable of measuring glucose concentration from the surrounding ISF. The external module has the function of feeding power to sensor and receiving the resonance frequency information via backscattered modulation. There is a high correlation between ISF glucose level and BGL. The dielectric constant of ISF changes when the BGL changes. This is reflected as a change in resonance frequency of the sensor. The ability of proposed sensor to track BGL was validated on live rodents in authorized clinical setting. The sensitivity of the proposed sensor has been evaluated in intravenous glucose tolerance test (IVGTT) on C57BL/6J mouse and insulin tolerance test (ITT) on *Sprague Dawley* rat. The sensor was designed, simulated, and optimized using an electromagnetic simulator supporting bio tissue models having similar dielectric permittivity with in vivo condition [29], [33].

II. Sensor Design, Simulation, Optimization and Evaluation

Enzyme-based glucose sensors require direct contact with blood or ISF to trigger an electrochemical reaction that produces a measurable physical quantity (current) in proportion with glucose level. However, the proposed EM-based sensor does not require direct contact with blood or ISF. Rather, the oscillating near field can sense minute changes in the dielectric permittivity of ISF owing to changes in glucose level. ISF and blood dielectric permittivity changes due to the change in blood glucose level [30], [34].

Glucose dependent *Cole-Cole* model for complex dielectric permittivity of blood plasma can be described as given in [53]:

$$\varepsilon(\omega,\chi) = \varepsilon_1(\omega,\chi) - j\,\varepsilon_2(\omega,\chi) = \varepsilon_\infty(\chi) + \frac{\Delta\varepsilon(\chi)}{1+\left(j\omega\tau(\chi)\right)^{\alpha}} \quad (1)$$

$$\varepsilon_1(\omega,\chi) = \varepsilon_\infty(\chi) + \frac{\Delta\varepsilon(\chi)}{1+(\omega\tau)^2}, \quad \varepsilon_2(\omega,\chi) = \frac{\Delta\varepsilon(\chi)*\omega\tau}{1+(\omega\tau)^2} \quad (2)$$

Where, $\varepsilon_1(\omega)$: frequency dependent dielectric constant, $\varepsilon_2(\omega)$: frequency dependent dielectric loss, χ is the concentration of analyte, $\Delta\varepsilon(\chi)$ is the magnitude of the dielectric dispersion that is the difference between static (ε_s) and high frequency (ε_∞) permittivity for analyte concentration, τ is the relaxation time, α is exponent for broadening of dispersion. In the present case, we are focusing detection of glucose from the ISF surrounding the implant sensor. The ISF is mostly composed of water which has dispersive dielectric behavior over frequency [62]. For instance, in case of water, the static and high frequency permittivity are ~79 and ~ 4.9 respectively with the relaxation frequency around 22 GHz. It can be seen that the dielectric loss factor is significantly high around this frequency. So, it would be wise not to design EM sensor around this frequency. In the lower *megahertz* frequency permittivity does not vary rapidly, however the loss factor is considerably higher compared to lower *gigahertz* frequency.

Similarly, the sensor embedded bio-environment (muscle and skin) has also dispersive dielectric nature. The dielectric dispersion of various biological tissue is summarized by Gabriel et. al in [29]. It is observed that dielectric permittivity of tissue varies rapidly in the *megahertz* frequency range, but not in g*igahertz* frequency range. In lower g*igahertz* frequency range bio tissue permittivity is almost stable. In the higher g*igahertz* frequency range, the development cost of integrated circuit and SoC system integration is a huge burden. Considering these facts, in the present work, we target to develop the sensor and system around 1~4 GHz frequency band.

A. Sensor modelling and sensing mechanism:

Sensors based on electromagnetic-induced transparency (EIT) can achieve ultra-high Q resonance capable for excellent sensing performance. EIT based sensors are realized for various applications covering sub-GHz band to THz frequency band [59]-[61]. An ultrahigh figure of merit at terahertz frequency is presented in [61], where metasurface supercell consists of slightly different ring resonators made of gold to achieve a high quality EIT resonance. In the present work, the sensor is a planar sinusoidal modulated resonator to achieve EIT–like transmission in the resonance window [50]. It utilizes localized energy confined to the sensor surface to detect small variations in the dielectric permittivity.

The sensor is intended to be implant type, so designing in the form of a cylindrical shape is most suitable for our case. Other forms of sensor like rectangular shapes have edges that will cause discomfort after implantation. Considering that, we chose flexible substrate material for our sensor. Polyamide substrate with $\varepsilon_r = 3.5$, $tan\delta = 0.002$ and thickness of 0.1 mm was used to simulate and fabricate the sensor. The cover layer of substrate was also removed in the fabricated samples to reduce rigidity and increase flexibility. The planar view and 3D model cut plane view of the sensor are shown in Fig. 2a and 2b respectively. The proposed sensor consists of one rectangular outer ring (11.6 mm x 14.6 mm) and one square inner ring (11 mm x 11 mm) placed over the same side of polyamide substrate (12 mm x 15 mm). The inner ring is coupled with the outer ring, and can be tuned to set the reference resonance frequency of the sensor. The outer ring is cut into two symmetric parts with the cut gap of 1.8 mm and excited directly using RF port. A capacitively coupled section in the shape of sinusoidally modulated pattern is placed inside the inner ring. The inner sinusoidally modulated pattern is defined as: $x(t) = k_0 * t; y(t) = k_1 * \sin(2 * \pi * k_2 * t)$,where k_0= 10.25, k_1= 5.54, k_2= 3.0, and t = (0, 1). The coupling section length is 3.5 mm and connects the modulation pattern at its end. Pair of this coupling sections are placed symmetrically at both end of modulation section inside inner ring. The modulation factor improves sensor impedance matching in a highly lossy dielectric environment and also improves sensor sensitivity. All the metallic traces are of 0.4 mm width, and with a copper thickness of 35µm. The planar sensor was wrapped around a Teflon (ε_r = 2.1, tan δ = 0.002) core having 3.8 mm outer diameter in the form of a cylinder as shown in Fig. 2b. Polyolefin material encloses the sensor and prevents bio material directly touching the sensor. In simulator, discrete lumped excitation port was defined at the two cut gap positions of outer ring, with one part as signal node and other part as ground node (Fig. 3a). The sensor is simulated as 2-port system having symmetric scattering parameters.

The packaging material encapsulating the sensor was also considered during simulation that isolates the sensor from the surroundings. Packaging material permittivity and thickness also affects the sensor resonance and sensitivity. A thicker packaging material with high dielectric permittivity holds most of the electric field from the sensor tightly within the material itself, hence sensor sensitivity decreases. The target was to achieve maximum sensitivity for a minute permittivity change around the sensor. Considering available options of packaging material and packaging process, polyolefin material was considered for fabrication. Polyolefin has the heat-shrinking properties that is suitable for our purpose. It has the unique characteristics of shrinking radially rather than longitudinally. At the same time, it offers good biocompatibility.

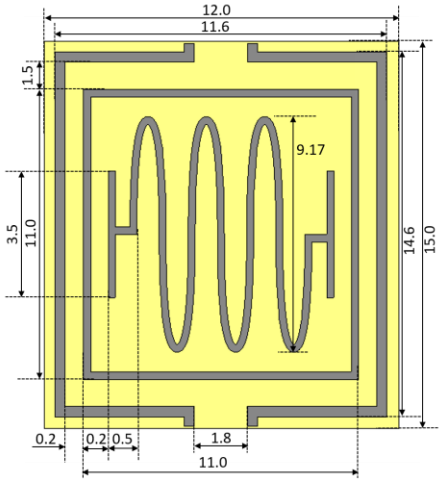

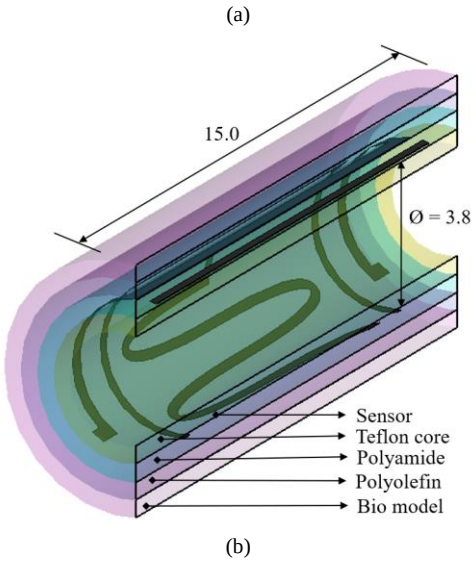

Fig. 2. Proposed EM-based implant glucose sensor: (a) Proposed sensor in planar form. (b) cut plane view of cylindrical implant sensor embedded within bio-tissue environment in simulator. (*Dimensions not to scale, unit: mm*)

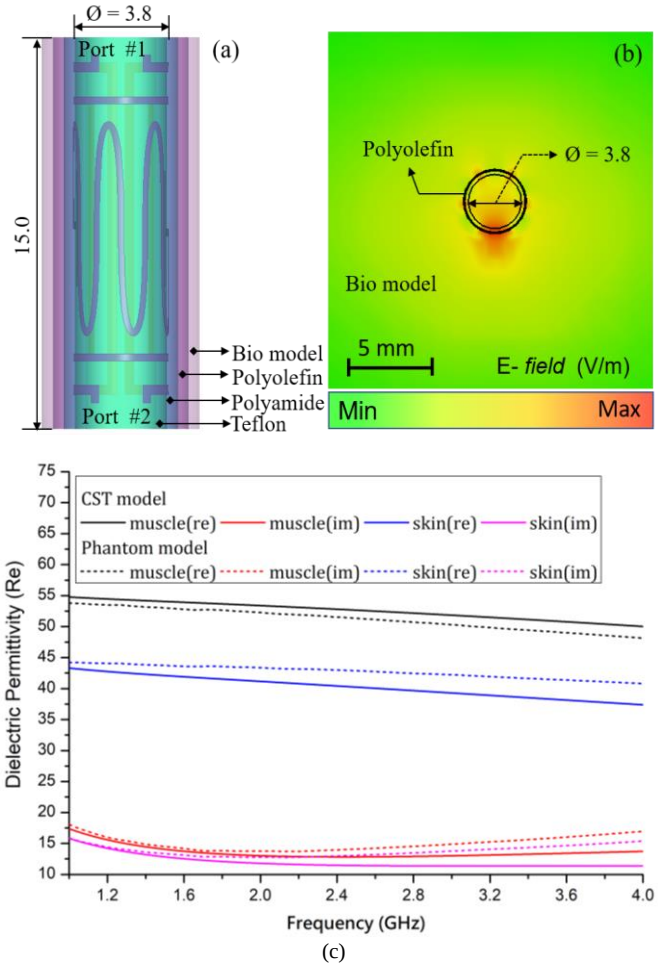

Fig. 3. (a) Sensor excitation port location (b) Simulated electric energy around the sensor inside bio-tissue environment, (c) dielectric properties of bio-tissue models of muscle and skin: bio model from EM simulator and in-house manufactured phantom model for the same

The sensor was simulated in a bio-tissue model supported in the electromagnetic simulator to check resonance behavior and optimize accordingly. Since the implant sensor will be inserted just below skin, it is necessary to consider skin and muscle environment to estimate resonance frequency of the sensor. The simulator provided a dispersive bio-model (Fig. 3c) that was considered to accurately simulate and optimize the sensor. To validate the sensor resonance behavior, we also manufactured phantom models mimicking skin and muscle properties as shown in Fig. 3c. The details of making phantom models similar to muscle and skin are described in *Section-II(D)*.

The sensor was modeled, simulated and optimized using CST microwave studio simulator. The scattering parameters of the sensor were analyzed over the frequency span of 1-4 GHz. In case of our implant sensor, the physical size of the sensor is much smaller compared to the wavelength at the resonance frequency. We used two different solvers i.e., transient and frequency domain solver to simulate and analyze the sensor resonance behavior. A fine meshing with high mesh density (30 mesh cells per wavelength) was adopted to accurately simulate the structure. The quality of discretizing/meshing is a tradeoff between simulation time, memory requirement and solution accuracy. Adaptive mesh refinement was also activated to ensure stability and consistency of sensor resonance in both transient (hexahedral mesh) and frequency domain (tetrahedral mesh) solvers. The boundary condition was set as *open* for both solvers. Critical design parameters (e.g., dimensions of rings and sinusoidal modulation pattern) were optimized using parametric analysis to ensure stable resonance in a lossy bio environment. A series of parametric analysis and optimization were done to maximize the sensitivity of the sensor towards minute dielectric permittivity variations.

B. Sensor packaging considerations and evaluation:

The proposed EM-based sensor is intended for subcutaneous implantation. Therefore, it is necessary to consider packaging material properties, e.g., physical strength, flexibility and shrinking ability, water proof nature, dielectric characteristics and biocompatibility characteristics. Biocompatible packaging can minimize/eliminate foreign body reactions [63]. Packaging material with high permittivity will hold most of the electric field within the package itself and restrict electromagnetic field interaction with surrounding material. Therefore, material with lower dielectric permittivity is suitable for present case. We considered polyolefin material for packaging of the sensor. It has low dielectric permittivity ~ 3.2 with low loss factor. This has the advantage of shrinking and adhering to the sensor surface's exact shape when applied with external heat treatment. Exposure to excessive heat generates micro cracks on the tube surface, which greatly affect the sensor performance during measurements. Thus, controlled heating at a lower temperature was adopted.

To maintain the sensor characteristics after inserting into a living body, it was necessary to prevent any kind of leakage that can cause shorting of the sensor terminals. The sensor was soldered to thin coaxial RF cables, and an extended polyolefin tube was used to cover the entire sensor and cable except SMA connector. The sensors were soaked in water for 24 hours to check any possible leakage in the packaging that could severely affect sensor performance. Usually, water absorbability is checked by measuring change in sample weight. However, we followed specific procedure to check water absorbability and leakage; we checked the change in resonance frequency. The

resonance frequency of the sensor before dipping into water and after removing from water (dried using cotton wipe) was the same. This ensured excellent hydrophobicity and leak-proof characteristics.

C. Sensitivity, SAR and RF safety Evaluation:

The proposed sensor is non-radiating with strong oscillating near field which enhances the dielectric sensing performance. Sensor sensitivity can be expressed as the amount of frequency deviation (Δf_r) from the reference frequency (f_r) due to small change in dielectric permittivity of surrounding material. Using perturbation theory, it can be expressed as the changes in the energy in a small volume (3).

$$\left|\frac{\Delta f_r}{f_r}\right| = \frac{\int_v^{v+dv}\left((\mu+\Delta\mu)|H_0|^2 + (\varepsilon+\Delta\varepsilon)|E_0|^2\right)dv}{\int_0^v\left((\mu)|H_0|^2 + (\varepsilon)|E_0|^2\right)dv} \quad (3)$$

where, 'v' represent the total volume of enclosing material (bio environment covering the entire sensor) in a close regime having the permittivity and permeability, as 'ε' and 'μ' respectively. Here we considered the reference permittivity (ε ~ 50) similar to the average permittivity of muscle and skin. The tissue environment has more like a dielectric characteristic (μ=1, $\Delta\mu$=0) than magnetic. The undisturbed electric and magnetic fields are represented as E_0 and H_0 respectively. In the proposed sensor, most of the field is confined at close proximity of sensor. The volumetric field variation due to small changes in permittivity (assuming Δε is due to glucose variation) in a small volume (dv) can be modelled as a small deviation in sensor frequency. The factor dv depends on the bio tissue thickness. The sensor sensitivity can also be affected by sample size/volume. We considered bio tissue with varying thickness 1~5 mm surrounding the sensor to check sensitivity variations. We observed the sensor resonance frequency was fairly unaffected by the volume of material surrounding the sensor. The confinement of electric field in the close proximity of the sensor surface resulted excellent sensitivity for thinner sample.

The proposed EM-based sensor is intended to be inserted subcutaneously below skin. Therefore, its effect on bio tissue is also important and must satisfy EM safety standards i.e., the specific absorption rate (SAR). This was numerically evaluated using full wave EM simulator CST Microwave studio. The SAR is defined as the time derivative of the incremental energy 'dw' absorbed by (or dissipated in) an incremental mass 'dm' contained in a volume element 'dv' of a given mass density 'ρ'.

$$\mathrm{SAR} = \frac{d}{dt}\left(\frac{\mathrm{d}w}{\mathrm{dm}}\right) = \frac{d}{dt}\left(\frac{\mathrm{d}w}{\rho.\,dv}\right) \quad (4)$$

$$\mathrm{SAR} = \left(\frac{\sigma.\,|\mathrm{E}|^2}{\rho}\right) \quad (5)$$

The SAR value is expressed in units of watts per kilogram (W kg $^{-1}$). Alternatively, it can be also calculated using equation (5) where E: electric field strength (rms) in tissue in V/m; σ: conductivity of body tissue in S/m; ρ: density of body tissue in kg/m^3. The simulator provided bio tissue model has density 1080 kg/m^3 and 1100 kg/m^3 for muscle and skin respectively. A dispersive dielectric model of 3rd order fit was the default condition in the simulation with conductivity of 0.79 S/m and 0.88 S/m of muscle and skin respectively.

In particular local SAR is more meaningful compared to the whole-body average SAR. The safety limits for SAR in U.S.A and Council of the European Union are 1.6 W/Kg (1-g tissue averaged) and 2.0 W/Kg (10-g tissue averaged), respectively. The proposed sensor can operate well with small input power. However, considering possible attenuation/loss in packaging material and bio tissue, power can be increased till the SAR within safe limit. In simulation, with an excitation of 15 dBm RF power, maximum SAR for proposed sensor is ~ 0.35 W/kg (1-g average). During the animal in vivo experiments, RF excitation power was set to 0 dBm or 1 mW in the network analyzer. This ensured highest safety measure considering SAR, and the sensor still showed good sensitivity even with this low power.

D. Phantom preparation mimicking bioenvironment:

This section describes steps of making phantoms mimicking muscle and skin tissue conditions [52]. The implanted sensor is intended to be located just below skin at an interface of skin and muscle tissue. In our work, we are focusing on lower *gigahertz* band and phantoms were prepared accordingly. At first the DI water was heated until the temperature reaches about 40 ℃. Maintaining DI water at same temperature, sodium chloride (NaCl) and sodium azide (NaN_3) were added with continuous stirring until dissolved. NaN_3 prevents the phantom from spoiling when exposed to room temperature and NaCl to ensure the conductivity requirement similar to the human body. Once NaCl and NaN_3 are completely dissolved, *Agar* powder (coagulant) was added slowly. It is important to observe the viscosity of solution and keep stirring so that the mixture should not become solid. Thereafter the mixture was heated up to 70 ^{0}C and TX-151 powder was added. After completely mixing TX-151 powder, polyethylene powder was added to the solution with continuous stirring. Small quantities of polyethylene powder should be added in multiple steps. Continuously stirring the solution ensures uniform permittivity throughout the phantom. Then the mixture was covered with plastic wrap kept for drying at room temperature for about a day.

TABLE. I BIO PHANTOM PREPARATION COMPOSITION: WEIGHT RATIO (%) OF CONSTITUENT MATERIALS FOR MAKING PHANTOM (MUSCLE, SKIN).

Ingredient	Bio Tissue Type	
	Muscle	Skin
DI-Water	74.51	81.5
NaN_3	0.04	0.05
TX-151	1.95	2.0
NaCl	0.55	0.6
Polyethylene	20.64	13.3
Agar	2.31	2.55
Total	100	100

In-house manufactured synthetic phantoms were used to check the sensor frequency and fluctuation level that we would expect during in vivo animal experiment. It also helped us to tune sensor design parameters to control the resonance frequency in an environment having similar permittivity level as in vivo. Differences in simulated and measured sensor resonance

characteristics were minimized by tuning and optimizing design parameters of the sensor. This helped to ensure a stable resonance within our targeted frequency band.

E. Sensitivity evaluation of sensor in continuous dielectric changes and aqueous glucose solutions: in vitro evaluation

This section explains the experimental setup and results to verify stability of the proposed sensor for continuous operation to track minute permittivity changes of embedded material. Considering temperature dependent dielectric permittivity of water, the proposed sensor was kept dipped in deionized (DI) water. As shown in Fig. 4(a), a temperature-controlled water bathtub (*C-WBD3, Changshin Science, Korea*) was used for heating and controlling the temperature of the water. DI water inside the tub can be heated quickly from normal temperature to user set temperature. After that it maintains the temperature of the DI water at that setting consistently. To cool down the water, the bathtub must be switched off. Therefore, it cools down at a relatively slower rate than it heats up in a typical room temperature condition. To maintain a uniform and stable temperature in the experiment, we placed another glass pot filled with DI water into the heating bathtub.

We used a small temperature sensor (34308-60001, *precision thermistor, Keysight*) dipped into the glass pot along with our sensor and a dielectric permittivity measurement probe (N1501A, *Performance Probe, Keysight*). Our sensor and permittivity measurement probe were connected to two different network analyzers. The temperature sensor (thermistor) was connected to a digital multimeter (34461A, *Keysight*) to show the temperature readings. The digital multimeter and two network analyzers were connected to a PC running automation program over LAN interface. The experimental setup continuously measured temperature of DI water, dielectric permittivity of DI water, and resonance frequency of the sensor dipped into the water (Fig. 4a). The measurement data were recorded using an in-house developed automation program with *Visual-C* programming language. Measurement data points were recorded at 1 sample per second rate.

As shown in Fig. 4b, the sensor resonance frequency changes following inverse relation with dielectric constant of DI water. The rate is similar between the dielectric change and sensor resonance frequency. After temperature of DI water reached maximum setting ~60˚C, the temperature was maintained for about 1-hour long. During that time no variations in sensor resonance frequency were observed. In the cooling down phase, the dielectric constant of the DI water slowly increased as the temperature decreased. The sensor resonance frequency was observed to decrease, obeying the inverse relationship with dielectric permittivity of water. The experiment was repeated several times on different days to ensure stability and repeatability. We observed total change in the dielectric permittivity of DI water and the total change in sensor resonance frequency while the temperature of the DI water varied from minimum (~21˚C) to maximum (~60˚C). From the measured data, the sensor showed about 4.1 MHz of frequency shift when the dielectric permittivity of DI water changes by one. A thicker packaging was used around the sensor because the sensor was kept at a high temperature for a long time inside the water during the experiment. This lowered the sensitivity and total frequency variation.

It was also confirmed that the sensor had no delay issues in responding to dielectric changes. This also ensured consistent performance in a continuous measurement scenario. The sensor response was fast and capable of accurately tracking small dielectric changes. It is important not to increase temperature too high that might affect the packaging material condition and adds noise to the sensor frequency response. The reason being, when we increased the temperature up to the boiling point of water, we observed moisture developed inside the sensor package tube. This affected sensor behavior severely and we observed fluctuation in sensor resonance frequency. This might be due to the possible development of microcracks on the packaging tube. So, we kept the temperature ~ 60 °C, much below the boiling point of water.

In vitro experiment to evaluate sensor sensitivity in aqueous glucose solution with varying glucose concentration was also done. The dielectric permittivity of glucose solution and the sensor resonance frequency were measured to understand sensor behavior and ability to detect glucose dependent permittivity changes. We prepared glucose solutions by adding exact amount of glucose (using a weighing scale) to DI water. Four different samples (90, 180, 270 and 360 mg/dL) were prepared with a realistic variation of BGL similar to humans. After preparing solutions, it was continuously stirred for 30 minutes using a magnetic stirrer inside sealed container. Then it was kept for 8 hours to make sample homogeneous in terms of glucose concentration and dielectric permittivity distribution. We measured the permittivity of the solutions using a performance probe (N1501A, Keysight) after calibrating the probe. During measurement the probe tip was checked carefully for possible presence of air bubbles after dipping into the solution. We observed dielectric permittivity of the solution decreases with increase in the glucose concentration (Fig. 4c). This trend is similar with the result reported in [53].

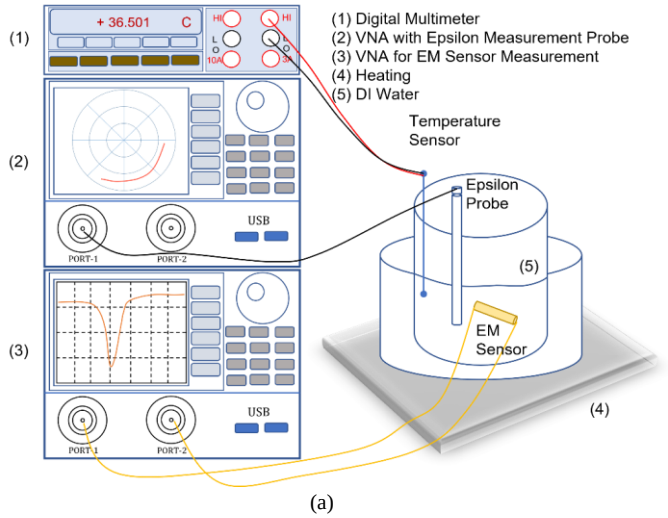

(a)

Measuring instruments used in the experiment:
1. Temperature sensor (34308-60001, *precision thermistor, Keysight*)
2. Digital multimeter (34461A, *Keysight*)
3. Material Measurement Kit (N1501A, *Keysight with Performance Probe*)
4. Vector network analyzer (E5071 *Keysight*)
5. ENA network analyzer (E5063A *Keysight*)
6. Hot water bathtub (C-WBD3, *Changshin Science, Korea*)

7. Desktop PC with automation program to record data continuously.

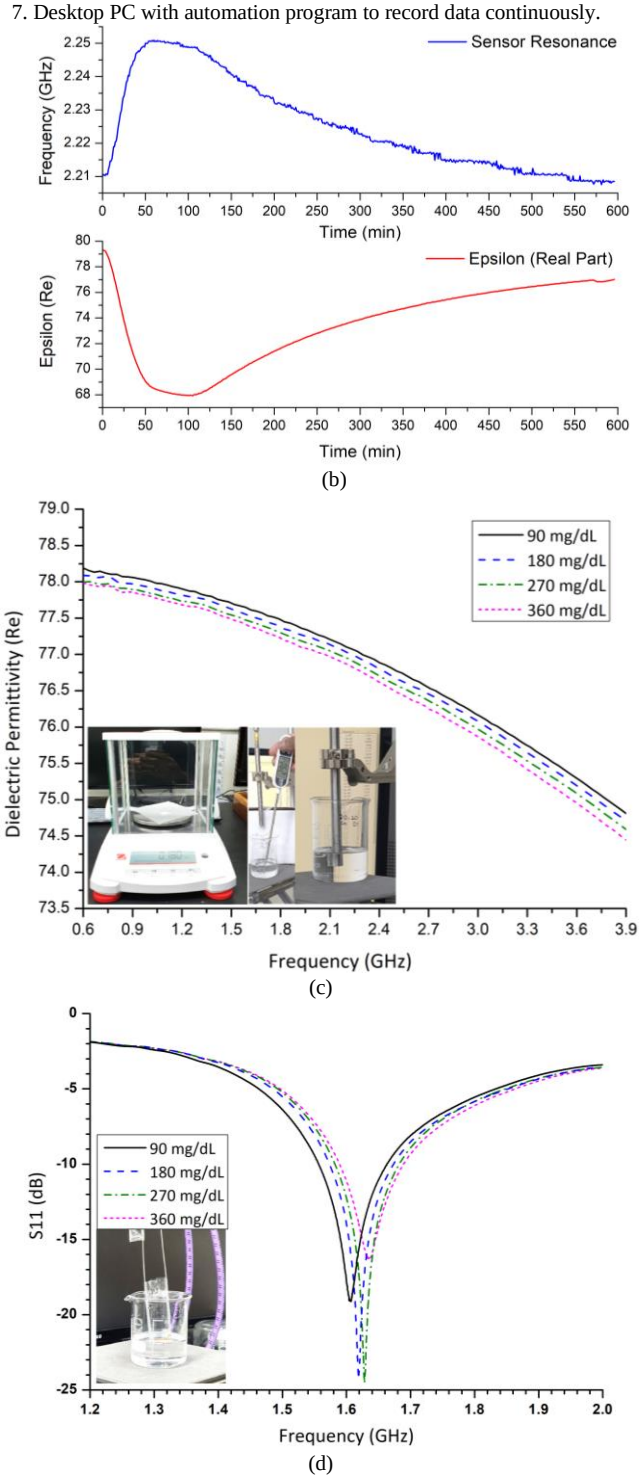

Fig. 4. (a) Experimental setup to check sensor sensitivity and capability to track continuous dielectric change, (b) Sensor resonance frequency inversely varying with water permittivity, (c) Permittivity of aqueous solution with different glucose concentration, (d) Sensor (thin package) frequency shift depending on glucose concentration in aqueous solution

The sensor with a thin packaging was used to check the sensitivity. The resonance frequency was measured after dipping the sensor in the glucose solutions. Each time the sensor was wiped and dried carefully before dipping into a glucose solution. It was observed that the sensor frequency increased with the increase in glucose concentration (Fig. 4d). The trend is consistent and in inverse relation with dielectric permittivity variation due to glucose concentration. The sensor frequency was observed to shift about ~29 MHz corresponding to a total variation of 270 mg/dL glucose level variation in the aqueous solution. It is important to maintain constant temperature of solutions during measurements to reduce temperature induce fluctuation effects.

III. MATERIALS AND METHOD

A. *Sensor fabrication and packaging:*

The sensor was fabricated using a flexible polyamide substrate. The flexible sensor was wrapped around a hollow Teflon core of 0.4 mm thickness. Using a hollow core helps us later to put the SoC and circuit inside the core. Thin metallic coaxial cable (*semi-rigid 034 cable assembly, 50 Ω*, Withwave) was soldered with the sensor port. The outer metallic conductor (ground) of the cable was also covered with same package tube (polyolefin, *Ace Tech Company*, Korea) so that there was no physical contact with the body of experimental animal during in vivo test. The complete sensor and coaxial cable were covered with packaging tube except the SMA connector part. During in vivo test, the sensor was inside the skin and suture was done to close the skin opening. The SMA connector was connected to the network analyzer using a high frequency cable.

To evaluate the proposed sensor's ability to track BGL, it is essential to understand how packaging material thickness can affect sensor performance. We considered two different cases of packaging thickness; first case, relatively thick (0.8 mm), second case, much thinner (0.2 mm). Fig. 5a shows fabricated and packaged sensors having two different material thickness. The dielectric permittivity of packaging material in both cases is same, hence the sensors had similar resonance frequency characteristics in air, as shown in Fig. 5b.

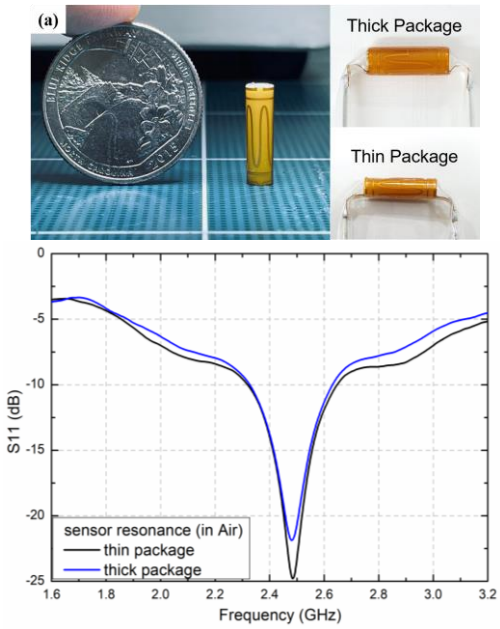

Fig. 5 (a) Picture showing sensor with two different packaging material, thick and thin, (b) Measured resonance characteristic of sensor with two different

type packaging thickness.

B. Animal model and materials used:

A C57BL/60J mouse from Jackson laboratory and Sprague Dawley rat were used in vivo evaluation of sensor. These experimental animals are widely used in various medical research focused on blood glucose [35]-[37]. The GTT was performed on the C57BL/6J mouse. Male mouse was chosen due to their better hormone stability, as suggested by veterinary doctor [40]. The fasting time for the mouse was approximately 12 h before the experiment [41]. The GTT was performed by injecting 20% glucose solution *(D-glucose Sigma-Aldrich*, Germany) through a tail vein of the mouse [42]. A catheter was used to inject the glucose solution into the vein. 10 µl of phosphate-buffered saline pH 7.4-1X (*Gibco*, USA) was injected into the tail vein before glucose administration. Approximately 0.2 ml (10 µl/g times animal body weight) glucose solution was intravenously injected [43]. The ITT was performed on Sprague Dawley rat. The experiment started from the initial condition of high BGL and injecting insulin to tail vein through a catheter, while the sensor was implanted at the abdomen below skin. After insulin was injected, both sensor frequency and BGL were observed at regular time internal. Catheter with a syringe filter (*Hyundai micro*, Korea) and 1-ml syringe (*26G ½, Becton, Dickinson*, USA) was used during the experiments.

C. In vivo experiment setup and preparations:

All preparations were done by a veterinary doctor following standard protocol for lab animal experiment before in vivo glucose test. Body weight and temperature were recorded for each animal subject. Dressing and hair removal from the skin at the sensor insertion site were performed. The skin layer on the abdominal cavity was cut, and the sensor was inserted into the body. It was observed that the implant site had small traces of blood in case of the rat, which was carefully cleaned. Any kind of clotting and drying of blood on sensor surface can affect sensor performance. In the case of the mouse, almost no blood was present at the sensor implant location. There was mostly ISF and body fluids around the sensor implant site. Suturing was performed to prevent the sensor coming out of the body. The breathing rate of the subject can introduce small movements in the sensor position. The surgery location was fixed using adhesive tapes to minimize measurement glitches due to movement of cables and sensor. Respiratory anesthesia was performed through the nose cap, and it was also fixed using tape to prevent any sudden movement of the animal. It was observed that the animal body temperature dropped after surgery and anesthetic injection [39]. During the experiment, temperature was maintained using the heating mat (*LSI HB 101/2*, USA). A digital temperature probe was inserted into the rectum of the animal to monitor body temperature continuously.

D. Anesthesia, BGL and sensor frequency measurement:

Measurements were planned to be performed with the sensor inserted into the animal body for few hours. Therefore, controlled anesthesia was performed before inserting the EM sensor and during the entire experiment period. A respiratory anesthesia method was used for the same. The ratio of the components of the breathing air was adjusted to 70% N_2O and 30% O_2. Isoflurane (*Terrell*, USA) was used as an anesthetic agent. Respiratory anesthesia was performed by mixing ~ 2% of the anesthetic in the air inhaled by the subject [38]. The concentration of the anesthetic agent was lowered to 1.5% after stabilized respiration.

The BGL was measured with a blood glucose meter (*Caresens-N, Korea*). BGL was tracked by taking a small amount of blood from tail vein of mouse/rat on a glucose measuring strip. Initially, measurement data (sensor frequency and BGL) were recorded every minute after glucose injection until we observed the glucose spike. After that, measurement data were taken at every 5 min until the BGL reduced to its initial level. A similar measurement procedure was followed in the case of the rat. Initially, BGL and sensor frequency were recorded every 2 min after insulin injection. After that, BGL data and sensor frequency were recorded every 5 min.

Sensor resonance characteristics were measured using network analyzer (*E5071, Keysight*, USA) during in vitro and in vivo experiments. Pair of high-frequency cables (s*emi-rigid 034 cable assembly 50 Ω, Withwave,* USA) were used to connect the sensor with the network analyzer. On the sensor side, the signal and ground terminals of the cable was soldered directly on the sensor excitation pads. The other side of the cable was connected to the network analyzer cable. To isolate cable length effect on the sensor performance, exact length of the cables was used for calibration of the network analyzer. Two port system calibration was done before each experiment. We tried to minimize any kind of cable twisting, movement during the in vivo experiments. After implantation of the sensor, its resonance frequency and corresponding blood glucose level of the animal were recorded at regular intervals of time.

Fig. 6. Mouse IVGTT experiment scenario and preparations (a) C57BL/6J mouse for IVGTT (b) Rectal thermometer insertion and respiratory anesthesia (c) Catheter insertion into tail vein (d) Hair removal and surgery (e) Insertion of sensor (f) Suture (g) Intravenous glucose injection (h) BGL measurement using *Caresens-N*

E. In vivo sensitivity evaluation of sensor with respect to BGL change:

In the animal experiments, the sensor was subcutaneously

inserted into the dermis layer directly below the skin. This has the advantage that pain receptors and nerves are not present in the dermis and subcutaneous fat layer [44]-[46]. It was observed that the sensor frequency changed according to the change in BGL during the in vivo GTT experiment. The sensor with thinner packaging had a lower resonance frequency and higher sensitivity compared to the sensor with thicker package. The reason being EM field is less attenuated in case of thin packaging, which improved the sensitivity of sensor.

Fig. 7. Rat ITT experiment scenario and preparations: (a) Sprague Dawley Rat for ITT (b) Rectal thermometer insertion and respiratory anesthesia (c) Catheter insertion into tail vein (d) Hair removal at the sensor implant position (e) Surgery for sensor implant (f) Insertion of sensor just below the skin (g) Suture and fixing sensor using tapes (h) Intravenous insulin injection and BGL measurement using *Caresens-N*

In the GTT experiment, a glucose solution (20% v/v) was injected into the tail vein of the mouse. In the ITT experiment, insulin (*Humalog*, 200 µl) was injected into the teil vein of the rat. In the GTT experiment, BGL was observed to increase rapidly after glucose injection. A few minutes after glucose injection, BGL was recorded at its maximum and then decreased slowly due to the natural action of body insulin. In the ITT experiment, BGL decreased from the maximum level after insulin administration. A consistent trend of increasing sensor frequency (moving to the higher side) with increasing BGL and decreasing sensor frequency (moving to the lower side) with decreasing BGL was observed during in vivo experiments. The trend is also consistent with in vitro results for aqueous glucose solutions. The detailed steps of the surgical insertions of the proposed sensor into mouse and rat are illustrated in Fig. 6 and Fig. 7, respectively. All the preparatory steps and surgery were performed by veterinary surgeon.

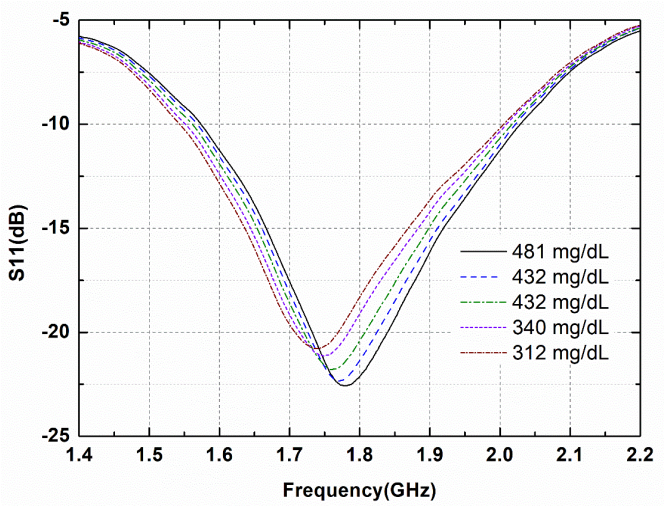

(a)

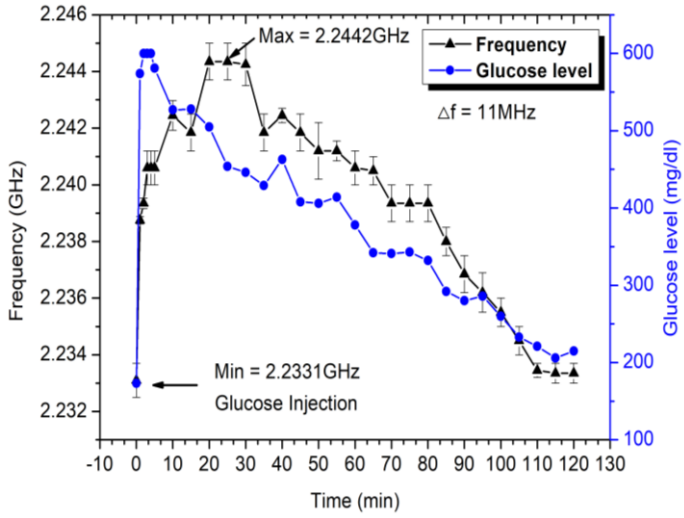

(b)

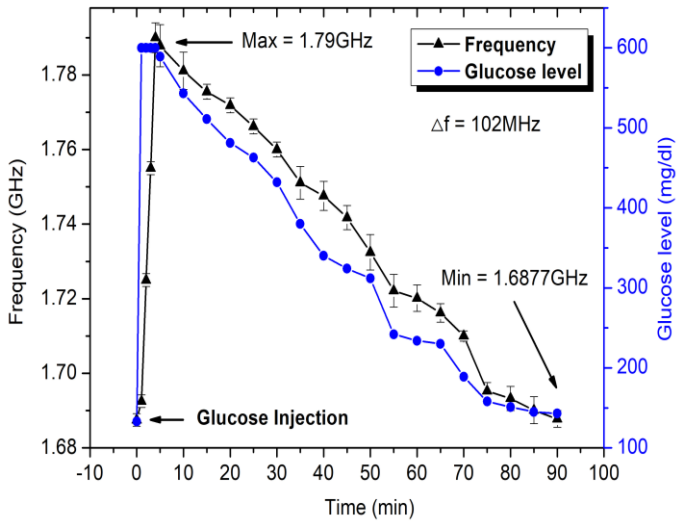

(c)

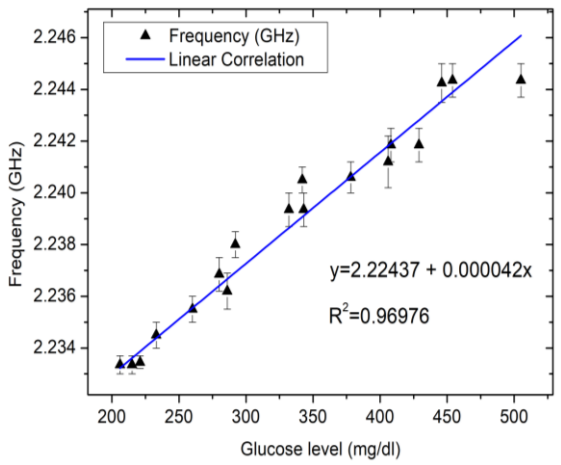

(d)

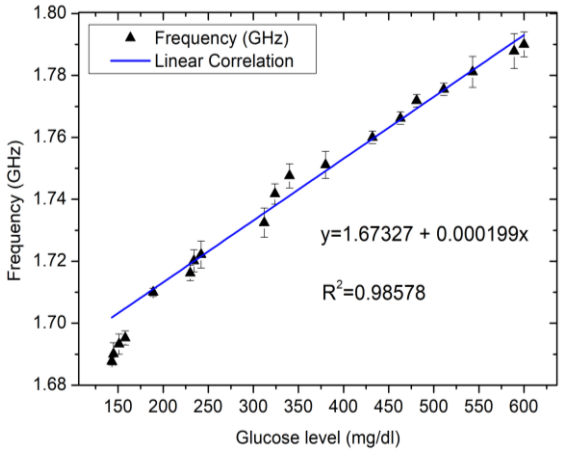

(e)

Fig. 8 (a) Sensor frequency variations with different BGL recorded for thin packaging. IVGTT on mouse showing sensor sensitivity with BGL change for (b) 0.8 mm (thick) and (c) 0.2 mm (thin) packaging. Linear regression correlation between sensor frequency and glucose level for sensor with (d) thick and (e) thin packaging.

We performed in vivo experiment on mouse with our sensor having two different packaging thicknesses, as described in the previous section. Due to the difference in package thickness and local permittivity at implant site in both cases, the sensor reference frequencies were also different. However, it was stable and showed good sensitivity towards BGL variations. The sensor resonance frequency at different BGL for thin package is shown in Fig. 8a. In case of sensor with thick packaging (Fig. 8b), the resonance frequency recorded at the time of glucose injection was 2.2331 GHz and increased to 2.2442 GHz. A total of 11 MHz frequency shift was observed in both the BGL increasing period (minimum to maximum after injection) and decreasing period (maximum to minimum due to natural insulin activation). After glucose injection, the BGL changed from 173 mg dl^{-1} to 600 mg dl^{-1} in the case of first mouse. The results of the sensor using thin packaging are shown in Fig. 8c. The BGL was observed to change from 133 mg dl^{-1} to 600 mg dl^{-1} after glucose injection in case of second mouse. The sensor frequency shift was observed to be considerably more in later case than that of former. The sensor resonance frequency increased from 1.6877 GHz to 1.79 GHz, which is approximately 102 MHz of frequency shift. From the IVGTT results for the mouse, it was found that the sensor with thin packaging had better sensitivity and a wider frequency shift compared to the thick packaging. Therefore, the sensor with thinner packaging was used in the ITT experiment on the SD rat. The sensor was implanted into the rat and insulin was administered. BGL was checked at regular intervals for 90 min. The BGL decreased from 305 mg dl^{-1} to 112 mg dl^{-1}. The sensor frequency decreased from 1.8925 GHz to 1.8420 GHz. Thus, a total frequency shift of 50.5 MHz was observed (Fig. 9a). The measured sensor resonance frequency trend in both packaging conditions was similar with the BGL change. In both GTT and ITT experiments, the sensor resonance frequency changed proportionally with the BGL change

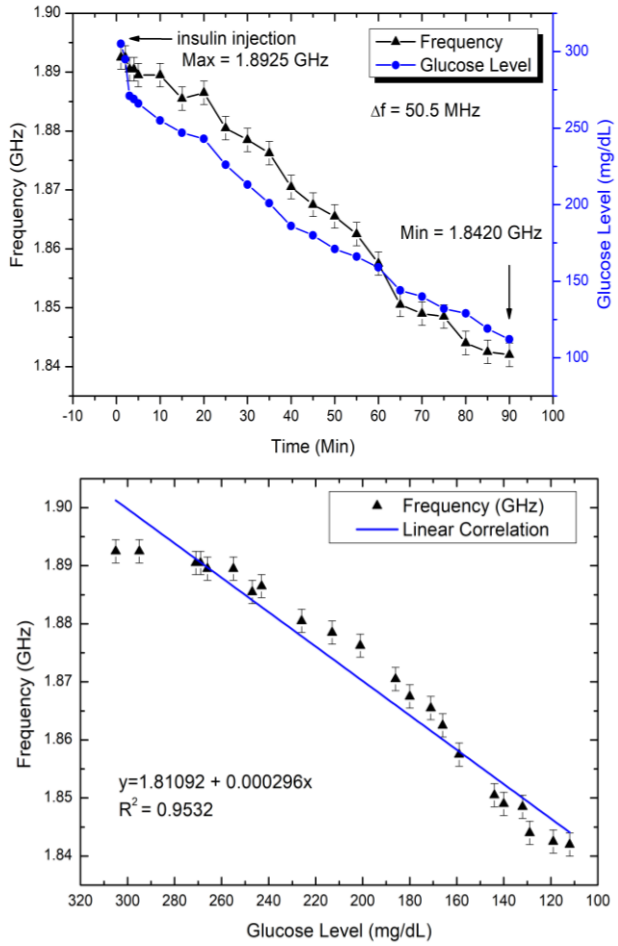

Fig. 9. Experimental results of ITT on SD rat, (a) resonance frequency change with BGL, and (b) linear regression correlation between sensor frequency and BGL.

The glucose from the blood capillary diffuses to the ISF surrounding tissues. So, there is a time delay between ISF glucose level and actual blood glucose level [47], [48]. This time delay between the peak BGL and peak ISF glucose level is usually about 10-20 minutes depending on the health condition of individuals. This time delay is an important parameter for predicting hyperglycemic or hypoglycemic alerts in continuous glucose monitoring systems (CGMS). Considering blood glucose trend with sensor calibration data, algorithm can be developed to improve time lag issue in calculating real time BGL and alert functions.

To map the sensor frequency to BGL, a linear regression model was used, which calculated the best linear fit between sensor frequency and BGL with minimum error for all measured data pairs. Linear correlation plots between sensor frequency and BGL in IVGTT experiment on mouse are shown in Fig. 8d and Fig. 8e for thick and thin packaging, respectively. The fitted linear regression for the ITT experiment on SD rat is shown in Fig. 9b for the thin packaging.

For the regression, we considered BGL decreasing event having data pairs of resonance frequency and corresponding BGL. The sensor with thick packaging ($R^2 = 0.9697$) showed a linear sensitivity of 41 kHz *per* 1-mg dl^{-1} of glucose change in the GTT. The sensor with thin packaging ($R^2 = 0.9857$) showed a linear sensitivity of 217 kHz *per* 1-mg dl^{-1} of glucose change in the GTT. In the ITT experiment, the sensor with thin packaging ($R^2 = 0.9532$) showed a linear sensitivity of 261 kHz *per* 1-mg dl^{-1} of glucose change. The above measured data and regression analysis indicates that our proposed implant sensor can effectively track BGL change with high accuracy. All the data are summarized in Table II. Real-time BG level can be obtained corresponding to a sensor frequency data using regression equation. Similarly, a change in BGL can be obtained from sensor frequency deviation.

TABLE II IN-VIVO EXPERIMENT SUMMARY. PROPOSED SENSOR SENSITIVITY IN IVGTT ON MOUSE AND ITT ON SD RAT.

Experimental species	Mouse	Mouse	Rat
Sensor Packaging	0.8 mm	0.2 mm	0.2 mm
Body weight (g) / age (weeks) / sex (M/F)	20.4 / 10 / M	21.1 / 9 / M	280 / 7 / M
Starting BGL to maximum BGL (mg/dL)	173 – 600	133 – 600	112 – 305
Sensor Resonance Frequency Shift (GHz)	2.2331 - 2.2442	1.6877 - 1.7900	1.8925 - 1.8420
Total Shift (MHz)	~ 11	~ 102	~ 50
Body temperature (^{0}C)	37 ± 0.3	37 ± 0.5	37 ± 0.5
Linear Regression *Y*: Frequency (GHz) *X*: BGL (mg/ dL)	$Y = 2.22437 + 0.000042\ X$	$Y = 1.67327 + 0.000199\ X$	$Y = 1.81092 + 0.000296\ X$
Linear correlation (R^2)	0.9697	0.9857	0.9532
Sensitivity (*per* mg. dl^{-1})	~ 41 kHz	~ 217 kHz	~ 261 kHz

IV. CONCLUSION

A fundamentally new approach for the development of EM-based glucose sensor capable of eliminating durability limitations inherent to enzyme-based and fluorescent-based sensors is presented. A durable, affordable, and reliable sensor for continuous glucose monitoring system can be realized using EM-based approach. For the same, development and initial in vivo evaluation of the sensor is discussed. To the best of our knowledge, proposed sensor is first of its kind subcutaneously implantable EM-based glucose sensor capable of continuously tracking real-time BGL. A few previously reported EM-based sensors have shown capability of continuous BGL tracking. Those sensors relied on changes in either phase or magnitude of scattering parameters according to BGL changes. However, the phase or amplitude variations are relatively small towards BGL variations. In the present case, the sensor resonance frequency changes significantly with minute changes in BGL. Detecting the relative shift in resonance frequency from a calibration point with respect to change in BGL is possible using regression model. An algorithm is also developed to reduce noise from the sensor data and calculate how much the sensor frequency moved from a reference point. It maps the difference in frequency to calculate corresponding changes in BGL, to estimate real-time BGL. Once-a-day calibration can be considered to set the reference point to minimize tracking/prediction error. Theoretically the electromagnetic behavior of the sensor does not degrade over time. However, there are various other factors that can potentially affect sensor performance. The sensor packaging is one important factor for long term use. Tissue inflammation, fibrous growth around sensor, biofouling, clotting of blood on sensor can severely degrade sensor performance over time. Packaging material with excellent biocompatibility can reduce foreign body reactions (FBR) around the sensor. The proposed sensor has been evaluated with live rodent animals (mouse and rat) in a clinically approved in vivo experiment. Excellent correlation between sensor frequency and blood glucose level is observed in IVGTT and ITT experiments.

ACKNOWLEDGMENT

Authors would like to thank veterinary surgeons of UNIST Animal Care and Use Committee. All experiments involving animals were approved by the Ulsan National Institute of Science and Technology, Animal Care and Use Committee (approval number: UNIST IACUC-19-32).

REFERENCES

[1] International Diabetes Federation Diabetes Atlas 9e EN, 201 (https://www.diabetesatlas.org/en/resources/)
[2] B. B. Lowell, and G. I. Shulman, "Mitochondrial Dysfunction and Type 2 Diabetes," Science, vol. 307, pp. 384–387, 2005
[3] Y. Yang, and W. Gao, "Wearable and flexible electronics for continuous molecular monitoring," Chemical Society Reviews, vol. 48, no. 6, 1465-1491, 2019.
[4] J. Kim, A.S. Campbell, and J. Wang, "Wearable non-invasive epidermal glucose sensors: A review," Talanta, vol. 177, pp. 163-170, 2018.
[5] Shibata, Hideaki, et al., "Injectable hydrogel microbeads for fluorescence-based in vivo continuous glucose monitoring," Proc. Natl. Acad. Sci. U.S.A., vol. 107, pp. 17894-17898, 2010.
[6] M. G. Ghosn et al., "Monitoring of glucose permeability in monkey skin in vivo using optical coherence tomography," J. Biophotonics., vol. 3, pp, 25–33, 2010.
[7] Larin, Kirill V et al., "Noninvasive blood glucose monitoring with optical coherence tomography: a pilot study in human subjects," Diabetes care, vol. 25, no. 12, pp. 2263-2267, 2002.
[8] E. Vezouviou, and C. R. Lowe, "A near infrared holographic glucose sensor," Biosens. Bioelectron., vol. 68, 371-381, 2015.
[9] L. B. Mohammadi et al., "In vivo evaluation of a chip based near infrared sensor for continuous glucose monitoring," Biosens. Bioelectron., vol. 53, pp. 99-104, 2014.
[10] B. Moore, "The Potential Use of Radio Frequency Identification Devices for Active Monitoring of Blood Glucose Levels," Journal of Diabetes Science and Technology, vol. 3, pp. 180-183, 2009.
[11] H. Park et al., "Radio frequency-based label-free detection of glucose," Biosens. Bioelectron., vol.54, pp. 141-145, 2014.
[12] N.Y. Kim et al., "A reusable robust radio frequency biosensor using microwave resonator by integrated passive device technology for quantitative detection of glucose level," Biosens. Bioelectron., vol. 67, pp. 687–693, 2015.
[13] X. Yang et al., "Direct molecule-specific glucose detection by Raman spectroscopy based on photonic crystal fiber," Anal. Bioanal. Chem., vol. 402, pp. 687–691, 2012.
[14] J.W. Kang et al., "Direct observation of glucose fingerprint using in vivo Raman spectroscopy," Sci. Adv., vol. 6, pp. eaay5206, 2020.

[15] S. Iguchi et al., "A flexible and wearable biosensor for tear glucose measurement," Biomed. Microdevices., vol. 9, pp. 603–609, 2007.
[16] A. Soni, and S. K. Jha, "A paper strip based non-invasive glucose biosensor for salivary analysis," Biosens. Bioelectron., vol. 67, pp. 763–768, 2015.
[17] W. Gao et al., "Fully integrated wearable sensor arrays for multiplexed in situ perspiration analysis," Nature, vol. 529, pp. 509–514, 2016.
[18] H. Lee et al., "A graphene-based electrochemical device with thermo responsive microneedles for diabetes monitoring and therapy," Nat. Nano technol., vol. 11, pp. 566–572, 2016.
[19] H. Lee et al., "wearable/disposable sweat-based glucose monitoring device with multistage transdermal drug delivery module," Sci. Adv., vol. 3, pp. e1601314, 2017.
[20] J. Kost et al., "Transdermal monitoring of glucose and other analytes using ultrasound," Nat. Med., vol. 6, pp. 347–350, 2000.
[21] H. Lee et al., "Enzyme-Based Glucose Sensor: From Invasive to Wearable Device," Advanced healthcare materials, vol. 8, pp. 1701150, 2018.
[22] E. Sehit, and Z. Altintas, "Significance of nanomaterials in electrochemical glucose sensors: An updated review (2016-2020)," Biosensors and Bioelectronics, vol. 159, pp. 112165, 2020.
[23] A. DeHennis et al., "An NFC-Enabled CMOS IC for a Wireless Fully Implantable Glucose Sensor," IEEE journal of biomedical and health informatics, vol. 20, pp. 18-28, 2015.
[24] J. Maddena et al., "Biosensing in dermal interstitial fluid using microneedle based electrochemical devices," Sensing and Bio-Sensing Research, vol. 29, pp. 100348, 2020.
[25] S. Xenofon et al., "A non-enzymatic glucose sensor enabled by bioelectronic pH control," Scientific reports, vol. 9, pp. 1-7, 2019.
[26] A.E. Colvin, and H. Jiang, "Increased in vivo stability and functional lifetime of an implantable glucose sensor through platinum catalysis," Journal of Biomedical Materials Research Part A, vol. 101A, pp. 1274-1282, 2013.
[27] P. Mehrotra, B. Chatterjee, and S. Sen, "EM-Wave Biosensors: A Review of RF, Microwave," mm-Wave and Optical Sensing Sensors, vol. 19, pp.1013, 2019.
[28] N.-Y. Kim et al., "Rapid, Sensitive and Reusable Detection of Glucose by a Robust Radiofrequency Integrated Passive Device Biosensor Chip," Scientific reports, vol. 5, pp. 1-9, 2015.
[29] S. Gabriel, R.W. Lau, and C. Gabriel, "The dielectric properties of biological tissues: III. Parametric models for the dielectric spectrum of tissues," Physics in medicine & biology, vol. 41, pp. 2271, 1996.
[30] E. Topsakal, T. Karacolak, and E.C.Moreland, "Glucose-dependent dielectric properties of blood plasma," XXXth URSI General assembly and scientific symposium, pp. 1-4 , 2011.
[31] S. Saha et al., "A Glucose Sensing System Based on Transmission Measurements at Millimetre Waves using Micro strip Patch Antennas," Scientific reports, vol. 7, pp. 1-11, 2017.
[32] K. Sasaki et al., "Measurement of the dielectric properties of the skin at frequencies from 0.5 GHz to 1 THz using several measurement systems," 2015 40th International Conference on Infrared Millimeter, and Terahertz waves (IRMMW-THz), Hong Kong, China, Aug, 23-28, 2015.
[33] D.-S. Yoo, "The dielectric properties of cancerous tissues in a nude mouse xenograft model," Bio Electro Magnetics, vol. 25, pp. 492-497, 2004.
[34] T. Karacolak, E. C. Moreland, E. Topsakal, "Cole–Cole model for glucose-dependent dielectric properties of blood plasma for continuous glucose monitoring," Microwave and optical technology Lett., vol. 55(5), pp.1160-1164, 2013.
[35] A.A. Toye et al., "A genetic and physiological study of impaired glucose homeostasis control in C57BL/6J mice," Diabetologia, vol. 48, pp. 675-686, 2005.
[36] G. Fergusson, et al., "Defective insulin secretory response to intravenous glucose in C57Bl/6J compared to C57Bl/6N mice," Molecular metabolism, vol. 3, pp. 848-854, 2014.
[37] A. Dudele et al., "Effects of ambient temperature on glucose tolerance and insulin sensitivity test outcomes in normal and obese C57 male mice," Molecular metabolism, vol. 3, no. 5, pp. e12396, 2014.
[38] C. Constantinides, R. Mean and B.J. Janssen, "Effects of isoflurane anesthesia on the cardiovascular function of the C57BL/6 mouse," ILAR journal/National Research Council, Institute of Laboratory Animal Resources, vol. 52, pp. e21-e31, 2011.
[39] Caro AC, Hankenson FC, and Marx JO, "Comparison of thermoregulatory devices used during anesthesia of C57BL/6 mice and correlations between body temperature and physiologic parameters," Journal of the American Association for Laboratory Animal Science, vol. 52, no. 5, pp. 577-583, 2013.
[40] H. J Goren, RN. Kulkarni, and C. R Kahn, "Glucose Homeostasis and Tissue Transcript Content of Insulin Signaling Intermediates in Four Inbred Strains of Mice: C57BL/6, C57BLKS/6, DBA/2, and 129X1," Endocrinology, vol. 145, no. 7, pp. 3307-3323, 2004
[41] S. Andrikopoulos et al., "Evaluating the glucose tolerance test in mice, "American Journal of Physiology Endocrinology and Metabolism, vol. 295, no. 6, pp. E1323-E1332, 2008.
[42] G. Frangioudakis et al., "The intravenous glucose tolerance test in cannulated Wistar rats: A robust method for the in vivo assessment of glucose-stimulated insulin secretion," Journal of pharmacological and toxicological methods, vol. 57, no. 2, pp. 106-113, 2008.
[43] G. Pacini, B. Omar and B. Ahrén, "Methods and Models for Metabolic Assessment in Mice," Journal of diabetes research, vol. 2013, ID986906, 2013.
[44] W. Groenendaal et al., "Quantifying the Composition of Human Skin for Glucose Sensor Development," Journal of Diabetes Science and Technology, vol. 4, no. 5, pp. 1032-1040, 2010.
[45] T. Graven-Nielsen and Sigfried Mense, "The Peripheral Apparatus of Muscle Pain: Evidence from Animal and Human Studies," The Clinical journal of pain, vol. 17, no. 1, pp. 2-10, 2001.
[46] M. Cherpi et al., "Nociception in the Skin: nociceptors are no longer the only actors," Douleur et Analgésie, vol. 32, pp. 217-220, 2019.
[47] T. Siegmund et al., "Discrepancies Between Blood Glucose and Interstitial Glucose—Technological Artifacts or Physiology: Implications for Selection of the Appropriate Therapeutic Target," Journal of diabetes science and technology 11.4, 766-772(2017).
[48] T. Koutny, "Blood glucose level reconstruction as a function of transcapillary glucose transport," Computers in biology and medicine, vol. 53, pp. 171-178, 2014.
[49] A. Caduff et al., "Non-invasive glucose monitoring in patients with Type 1 diabetes: A Multi sensor system combining sensors for dielectric and optical characterization of skin," Biosensors and Bioelectronics, vol. 24, pp. 2778-2784, 2009.
[50] J. Malik et al., "Electromagnetically induced transparency in sinusoidal modulated ring resonator," Appl. Phys. Lett., vol. 112, pp. 234102, 2018.
[51] J. Hanna et al., "Noninvasive, wearable, and tunable electromagnetic multi sensing system for continuous glucose monitoring, mimicking vasculature anatomy" Sci. Advances., vol. 6, no. 24, pp. eaba5320, 2020.
[52] J.H. Choi et al., "RF Characteristics Semi-Solid Body Phantom Manufacturing Method and Body Phantom Manufacturing Components," KR Patent 10-2013-0076784, Step. 14, 2014.
[53] M. Hays et al., Glucose-dependent dielectric Cole-Cole models of rat blood plasma from 500 MHz to 40 GHz for millimeter-wave glucose detection, Microwave Opt. Tech. Lett., vol. 62, pp. 2813-2820, 2020.
[54] A. E. Omer et al., "Blood Glucose Level Monitoring Using an FMCW Millimeter-Wave Radar Sensor," Remote Sensing, vol. 12, no. 3, p. 385, Jan. 2020.
[55] G. Shaker et al., "Non-Invasive Monitoring of Glucose Level Changes Utilizing a mm-Wave Radar System. International Journal of Mobile Human Computer Interaction, vol. 10(3), pp. 10-29, 2018.
[56] H. Cano-Garcia et al., "Millimeter-wave sensing of diabetes-relevant glucose concentration changes in pigs," J. Infrared, Millimeter, Terahertz Waves, vol. 39, no. 8, pp. 761–772, Aug 2018.
[57] S. Y. Huang et al., "Microstrip Line-Based Glucose Sensor for Noninvasive Continuous Monitoring Using the Main Field for Sensing and Multivariable Crosschecking," in IEEE Sensors Journal, vol. 19, no. 2, pp. 535-547, 15 Jan.15, 2019.
[58] H. Cano-Garcia, P. Kosmas, et al, "Detection of glucose variability in saline solutions from transmission and reflection measurements using V-band waveguides," Measurement Science and Technology, vol. 26, no. 12, 125701, 2015.
[59] F. Gao et al., "Active Electromagnetically Induced Transparency Effect in Graphene-Dielectric Hybrid Metamaterial and Its High-Performance Sensor Application" Nanomaterials, 2032(11), 2021.
[60] C. Huang et al., "An Electromagnetically Induced Transparency Inspired Antenna Sensor for Crack Monitoring," IEEE Sensors Journal, vol. 21, no. 1, pp. 651-658, 1 Jan.1, 2021.
[61] I. Al-Naib, "Electromagnetic-Induced Transparency Resonance with Ultrahigh Figure of Merit Using Terahertz Metasurfaces," Journal of Infrared, Millimeter, and Terahertz Waves, 42, 4, (371-379), 2021.
[62] A. Caduff et. al., "Continuous noninvasive glucose monitoring; water as a relevant marker of glucose uptake in vivo," Biophysical Reviews, vol. 11, pp. 1017–1035, 2019.
[63] A.K. Means et al., A self-cleaning, mechanically robust membrane for minimizing the foreign body reaction: towards extending the lifetime of sub-Q glucose biosensors. J Mater Sci Mater Med., 30(7), 79, 2019.